Received: 15 September 2019 | Revised: 16 January 2020 | Accepted: 20 February 2020

DOI: 10.1002/gj.3807

WILEY

SPECIAL ISSUE ARTICLE

Quantitative critique of leaf-based paleo-CO_2 proxies: Consequences for their reliability and applicability

Wilfried Konrad[1,2] | Dana L. Royer[3] | Peter J. Franks[4] | Anita Roth-Nebelsick[5]

[1]Department of Geosciences, University of Tübingen, Tübingen, Germany

[2]Institute of Botany, Technical University of Dresden, Dresden, Germany

[3]Department of Earth and Environmental Sciences, Wesleyan University, Middletown, Connecticut

[4]Faculty of Agriculture and Environment, The University of Sydney, Sydney, New South Wales, Australia

[5]State Museum of Natural History Stuttgart, Stuttgart, Germany

Correspondence
Wilfried Konrad, Department of Geosciences, University of Tübingen, Tübingen, Germany.
Email: wilfried.konrad@uni-tuebingen.de

Funding information
National Science Foundation, Grant/Award Number: OCE-16-36005; The Australian Research Council

Peer Review
The peer review history for this article is available at https://publons.com/publon/10.1002/gj.3807.

Handling Editor: T. Utescher

A variety of proxies have been developed to reconstruct paleo-CO_2 from fossil leaves. These proxies rely on some combination of stomatal morphology, leaf $\delta^{13}C$, and leaf gas exchange. A common conceptual framework for evaluating these proxies is lacking, which has hampered efforts for inter-comparison. Here we develop such a framework, based on the underlying physics and biochemistry. From this conceptual framework, we find that the more extensively parameterised proxies, such as the optimisation model, are likely to be the most robust. The simpler proxies, such as the stomatal ratio model, tend to under-predict CO_2, especially in warm (>15°C) and moist (>50% humidity) environments. This identification of a structural under-prediction may help to explain the common observation that the simpler proxies often produce estimates of paleo-CO_2 that are lower than those from the more complex proxies and other, non-leaf-based CO_2 proxies. The use of extensively parameterised models is not always possible, depending on the preservation state of the fossils and the state of knowledge about the fossil's nearest living relative. With this caveat in mind, our analysis highlights the value of using the most complex leaf-based model as possible.

KEYWORDS
CO_2, leaf gas exchange, palaeoclimate, proxy, stomatal ratio, $\delta^{13}c$

1 | INTRODUCTION

1.1 | Motivation

For over three decades, the often observed negative correlation between stomatal density and atmospheric CO_2 concentration (Woodward, 1987) has been utilised as a plant-based proxy for obtaining palaeo concentrations of CO_2. Accordingly, different approaches to using fossil stomatal data to calculate CO_2 levels of the past have been developed during that time. Stomatal data are now a standard proxy to be included in data synopses summarising available proxy information on CO_2 development (Anagnostou et al., 2016; Foster, Royer, & Lunt, 2017).

Simultaneously, substantial research efforts were dedicated to the effects of (mostly elevated) CO_2 on gas exchange of extant plants to obtain a solid data basis for predicting and modelling the impact of anthropogenic CO_2 increase on terrestrial vegetation [see reviews by Ainsworth and Rogers (2007) and Franks et al. (2013)]. Stoma-based proxy approaches for reconstructing palaeo-CO_2 benefitted from these studies (e.g., Franks et al. (2014); Konrad, Katul, Roth-Nebelsick, and Grein (2017); Konrad, Roth-Nebelsick, and Grein (2008)).

Principally, the relationship between stomatal density and CO_2 is tackled with two different concepts.

- The first (and older) approach applies the phenomenological concept which utilises collected data pairs, comprising stomatal density and CO_2, to construct a curve of CO_2 vs. density to serve as a basis for calculating CO_2 from fossil stomatal density. The fact that stomatal density is also influenced by environmental conditions other than CO_2 concentration was acknowledged early, and the remedy was to replace stomatal density with the stomatal index, which is—in extant plants—much less affected by humidity or other 'non-CO_2' factors. (Stomatal index is the ratio of stomatal density to stomatal plus epidermal cell density, expressed as a percentage.)
  Over time, a number of 'best practise' recommendations accumulated, such as a minimum of cuticle area used for counting stomata (Poole, 1999) and more appropriate statistical methods (Beerling & Royer, 2002). The phenomenological concept can be further subdivided into two approaches. With the 'full calibration' approach, a number of data pairs (stomatal density or index plus CO_2) is collected and a continuous curve is erected via curve fitting (Barclay & Wing, 2016; Kürschner, van der Burgh, Visscher, & Dilcher, 1996; Wagner et al., 1996). The second approach is termed 'Stomatal Ratio' and is based on the observation that the ratio of stomatal densities or stomatal indices developing under different CO_2 concentrations is reciprocal to the ratio of these different CO_2 concentrations (McElwain & Chaloner, 1995, 1996; Steinthorsdottir & Vajda, 2015). Another plant-based, phenomenological proxy is that from Schubert and Jahren (2012, 2015) (see also Cui & Schubert, 2016). Here, the ratio between plant internal CO_2 concentration (C_i) and external (atmospheric) CO_2 (C_a), as derived from $\delta^{13}C$ of fossil plant material, is utilised. Although not explicitly stomatal-based, this approach is included because it is related to plant gas exchange.
- Mechanistic approaches, in contrast, derive a relation between C_a and leaf traits from established physics (such as diffusion) and physiological processes (such as photosynthesis) supplemented by principles of stomatal regulation. Optimisation models [e.g., Cowan (1977), Katul, Palmroth, and Oren (2009), and Konrad et al. (2008)] and similar approaches [e.g., Franks et al. (2014) and Konrad et al. (2017)] belong to this class.

The aim of this contribution is to illustrate shared similarities and differences between the various approaches from the viewpoint of their emerging mathematical structure and physical/physiological background, and to evaluate their applicability and reliability as limited by different conditions (cf. Figure 1).

This review aims to identify the skeleton of a 'parent' model which underlies—implicitly or explicitly—all approaches and further approximations and/or auxilliary assumptions (often tacitly made) which distinguish the various methods. On the basis of these differences, aspects will be discussed with respect to applicability and reliability of the various paleo-CO_2 reconstruction approaches [how much information/how many parameters have to be known from independent sources, how feasible are certain approximations (e.g., the question of leaf temperature)].

1.2 | A summary of physical and physiological mechanisms of stomatal sensitivity to CO_2

The CO_2 sensitivity of stomata is ultimately caused by photosynthesis and its coupling with transpiration and therefore lies at the basis of all stomata-related proxy methods. At the leaf-scale, the basic physiological processes and physical laws are described by:

- The Farquhar photosynthesis model describing the biochemical demand of CO_2 (Farquhar, von Caemmerer, & Berry, 1980, 2001) for C_3-plants given as:

$$A = q\,\frac{C_i - \Gamma}{C_i + K} - R_d, \tag{1}$$

where A is leaf net photosynthetic assimilation (i.e., photosynthesis minus leaf autotrophic respiration), q denotes carboxylation limited

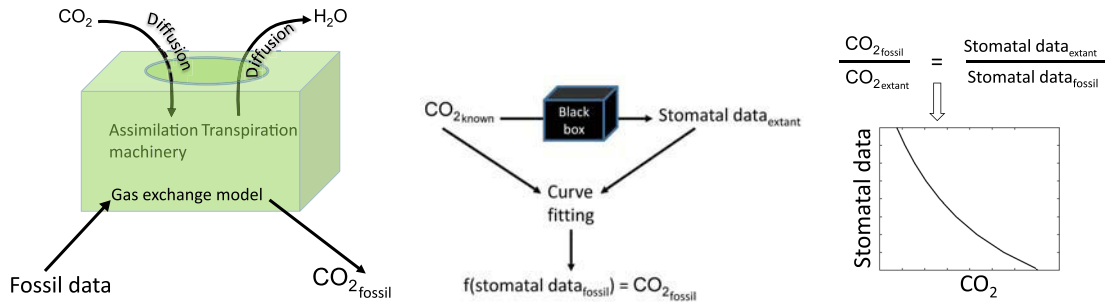

(a) Mechanistic approach (b) Transfer function approach (c) Stomatal ratio approach

FIGURE 1 Both mechanistic and phenomenological approaches of paleo-CO_2 reconstruction are based on the laws of physics and biochemistry. (a) Mechanistic approaches formulate the interactions between the relevant quantities explicitly in terms of mathematical models. Phenomenological approaches, in contrast, (b) either stow away the physiological machinery in a black box that remains unexplored or (c) postulate instead that ratios of CO_2-values are reciprocally equal to the ratios of the related stomatal quantities [Color figure can be viewed at wileyonlinelibrary.com]

by Rubisco or RuBP regeneration rate, K is a parameter containing Michaelis–Menten constants of carboxylation and oxygenation, Γ is the CO_2 compensation point and R_d is the mitochondrial respiration rate. Equation (1) is to be understood to describe the smaller of two potential rates of carboxylation: limitation by RuBP or by Rubisco regeneration. In the first case, $q = J/4$, where J is the rate of electron transport (which depends on the absorbed solar photosynthetic active radiation), while in the second case it is equal to maximum carboxylation velocity, that is, $q = V_{c,\,\max}$. For the structural considerations that will be discussed in what follows it is not necessary to know which alternative is realised in a specific case. Limitation of RuBP regeneration occurs under lower solar irradiances, when the stomata are not fully open. In this phase, stomatal conductance is hence regulated by the opening of the stomata, and not by a change in their density. Density regulation thus appears to be important in the Rubisco-limitation phase, when the stomata tend to be fully or almost fully open. Hence, it is $q = V_{c,\,\max}$, and not $q = J/4$, which is important in this study focussing on stomatal density and stomatal index. The dependence of the biochemical parameters q, Γ, K and R_d on air temperature T is described by relations derived elsewhere (Bernacchi, Pimentel, & Long, 2003).

When borrowing q from extant plants, an uncertainty range has to be considered which is caused by natural variation and also some environmental influences. For example, leaf nutrient status affects q to some degree. Also, C_a itself may modulate q, as indicated by experimental data (Ainsworth & Rogers, 2007). It is, however, difficult to assess this effect for geological time scales for fossil plants which were adapted to the palaeo-C_a level. It is generally recommended to conduct a systematic parameter variation covering the variability range of $V_{c,\,max}$ and to clearly state and discuss sources and ranges of uncertainty when working with values borrowed from extant plants.

- Fick's law of diffusion describing the atmospheric supply of CO_2 into and loss of water from the intercellular space. Assimilation rate A and transpiration rate E read:

$$A = g\ (C_a - C_i), \tag{2}$$

$$E = ag\ (w_{sat} - w_a), \tag{3}$$

where g is leaf conductivity with respect to CO_2, C_i is the leaf internal CO_2 concentration, w_{sat} is the leaf internal air humidity (taken as the saturation value for water vapour concentration in air), and w_a is the leaf external air humidity. The parameter $a = D_{H_2O}/D_{CO_2} = 1.6$ is the ratio of the diffusional constants of water vapour and CO_2 in air. For stationary conditions (i.e., all CO_2-molecules diffusing into the leaf interior are finally assimilated), the biochemical demand and atmospheric supply of CO_2 must be in balance. This assumption is employed throughout.

- In order to end up with manageable equations, the complex arrangement of cells and voids inside the real leaf has to be approximated by simpler structures. Various approaches have been developed [Aris (1975); Brown and Escombe (1900); Parlange and Waggoner (1970); for a review see Parkhurst (1994)]. Here, we use the porous medium approximation (Aris, 1975; Konrad et al., 2008; Parkhurst, 1994) which replaces the real leaf by a fictitious tissue which is characterised by just two quantities, the porosity n and the tortuosity τ. Application of the diffusion law to this simplified tissue provides a relation between leaf conductance g and stomatal density ν and other leaf anatomical parameters:

$$\nu = \frac{g\ d_{st}}{\left(D_{CO_2} - g\left[d_{bl} + d_{as}\frac{\tau_{as}^2}{n_{as}}\right]\right)a_{st}}, \tag{4}$$

where d_{as}, τ_{as}, and n_{as} are thickness, tortuosity and porosity of the assimilation layer, a_{st} and d_{st} are cross-sectional area and depth of the stoma, and ν is the stomatal density. d_{bl} is the thickness of the laminar boundary layer attached to the leaf surface, whose thickness depends on leaf size l and wind speed v_{wind}, approximately according to $d_{bl} \approx 4 \times 10^{-3}\mathrm{m}/\sqrt{s}\sqrt{l/v_{wind}}$.

If g can be expressed as a function of C_a and the photosynthesis parameters q, K, Γ, R_d (which we assume to be known), Equation (4) provides a relation between ν and C_a that can be used to reconstruct palaeo-CO_2 from fossil leaf anatomy.

2 | BASIS AND STRUCTURE OF THE CONSIDERED APPROACHES

We will start with the mechanistic models. Equations (1) and (2) represent only two relations for the three variables g, A and C_i. Hence, a third relation is required. The various mechanistic models follow different strategies to obtain the missing relation:

1. The optimisation models translate the strategy of plants to gain a maximum of carbon with a given amount of available water (while the variations of the environmental factors are also taken into account) into the mathematical language of optimisation principles (Aalto & Juurola, 2002; Berninger, Mäkela, & Hari, 1996; Buckley & Schymanski, 2014; Cowan, 1977; De Boer et al., 2011; Katul et al., 2009; Katul, Manzoni, Palmroth, & Oren, 2010; Konrad et al., 2008; Way, Oren, Kim, & Katul, 2011). This yields an additional algebraic relation for g in terms of the environmental and photosynthetic parameters.
2. Most of the other models [e.g., Franks et al. (2014) and the 'reduced order model' of Konrad et al. (2017)] restrict their model dynamics to carbon balance of the fossil leaf. They obtain the missing information on leaf conductance from determining C_i/C_a, based on the well-known fact that both diffusion and photosynthesis discriminate between ^{12}C and ^{13}C carbon isotopes. Exploiting this fact, it is possible to calculate the ratio:

$$\kappa = \frac{C_i}{C_a}, \tag{5}$$

from $\delta^{13}C$ data from fossilised leaves (Beerling, 1994; Diefendorf, Freeman, Wing, Currano, & Mueller, 2015; Farquhar, O'Leary, & Berry, 1982; Grein, Roth-Nebelsick, & Wilde, 2010).

2.1 | Mechanistic approaches

2.1.1 | Optimisation models

Adopting the nomenclature used in Konrad (2007) and Konrad et al. (2008) the optimisation approach can be summarised as follows:

- C_i is expressed in terms of the biochemical parameters q, Γ, K and R_d and the conductivity g by equating the right-hand sides of expressions (1) and (2). This results in a quadratic equation for C_i with solutions:

$$C_i = \frac{1}{2g}\{g(C_a - K) - (q - R_d) \pm \sqrt{[g(C_a - K) - (q - R_d)]^2 + 4g(gKC_a + q\Gamma + KR_d)}\}. \quad (6)$$

(The solution with the minus sign in front of the square root symbol leads to negative C_i and should therefore be ignored.) Substitution into Equation (2) yields an assimilation rate:

$$A = \frac{1}{2}\{g(C_a + K) + (q - R_d) - \sqrt{[g(C_a - K) - (q - R_d)]^2 + 4g(gKC_a + q\Gamma + KR_d)}\}. \quad (7)$$

A is thus expressed in terms of leaf conductivity g as well as the photosynthetic parameters (q, K, Γ, R_d) and C_a.

Notice that in Equation (3) the transpiration rate E is also expressed in terms of leaf conductivity g.

- Plants maximise their assimilation in a manner that accounts for diurnal or even seasonal changes in environmental factors such as air temperature, humidity and irradiance. This maximisation is achieved by varying leaf conductance g (by adjusting stomatal area a_{st} to the diurnal variations of the environmental factors or by adjusting stomatal density ν as response to seasonal changes, or both). The task is therefore to find the g that maximises assimilation for finite transpiration while taking into account prescribed changes of temperature, humidity and irradiance. The mathematical technique by which this goal is achieved is the calculus of variation with constraints. According to this technique, the statements:

$$\int_{\Delta t} A(g(t))\, dt = \text{maximum} \quad \text{and} \quad \int_{\Delta t} E(g(t))\, dt = W_0 \quad (8)$$

have to be fulfilled simultaneously, where Δt is a preset time span over which the optimization is sought (e.g., one day or one season). The second relation represents a constraint: W_0 denotes the amount of water (per leaf area) that the plant may transpire during Δt. It is furthermore understood that the quantities w_a, q, Γ, K and g appearing in expressions (1), (2) and (3) for E and A depend either explicitly on time t or implicitly via a time-dependence (diurnal course) of air temperature, $T(t)$.

- The optimisation procedure by which g is calculated starts with forming the expression:

$$L = A - \lambda E = \frac{1}{2}\left\{g(C_a + K) + (q - R_d) - \sqrt{[g(C_a - K) - (q - R_d)]^2 + 4g(gKC_a + q\Gamma + KR_d)}\right\} - \lambda\, ag(w_{sat} - w_a), \quad (9)$$

where the second expression is derived when substituting A and E by expressions (7) and (3). (In mathematical terminology, L is the Lagrangian and the arbitrary constant λ is the Lagrange multiplier and $\int_{\Delta t} E(t)\ dt = W_0$ is the constraint of the problem.) The calculus of variation transforms the constrained optimization problem above into an unconstrained one in which L can be obtained from solving the following ordinary differential equations:

$$\frac{d}{dt}\frac{\partial L}{\partial \dot{g}} = \frac{\partial L}{\partial g}, \quad (10)$$

where $\dot{g} \equiv \frac{dg}{dt}$. The last equation constitutes an ordinary differential equation of second order for the conductance $g(t)$. In the last step, λ is calculated by evaluating the constraint $\int_{\Delta t} E(g(t))\ dt = W_0$ with the help of the now known conductance $g(t)$.

Inspection of expressions (7) and (3) shows that both A and E depend on g but neither of them depends on $\dot{g}$. Hence, Equation (10) reduces to:

$$0 = \frac{\partial L}{\partial g}. \quad (11)$$

This finding allows two important simplifications: (a) The differential Equation (10) of the generic case reduces to an algebraic equation for $g(t)$, and, (b) to solve Equation (11) for $g(t)$ the time dependencies of the quantities w_a, q, Γ, K and R_d need not be known explicitly.

Application of the optimisation scheme to Equation (9) results in:

$$g = \frac{1}{(C_a + K)^2}\left[\sqrt{\frac{q\,(K + \Gamma)[C_a(q - R_d) - (q\Gamma + KR_d)]}{[C_a + K - \lambda a(w_{sat} - w_a)]\lambda a(w_{sat} - w_a)}}\,[C_a + K - 2\lambda a(w_{sat} - w_a)] + (q - R_d)\,C_a - (q\Gamma + KR_d) - q\,(K + \Gamma)\right] \quad (12)$$

and after insertion into (7) and (3),

$$A = \frac{1}{(C_a + K)}\left[C_a(q - R_d) - (q\Gamma + KR_d) - \sqrt{\frac{q\,(K + \Gamma)[C_a(q - R_d) - (q\Gamma + KR_d)]\lambda a(w_{sat} - w_a)}{(C_a + K - \lambda a(w_{sat} - w_a))}}\right] \quad (13)$$

and

$$E = \frac{a(w_{sat}-w_a)}{(C_a+K)^2}\left[\sqrt{\frac{q\ (K+\Gamma)[C_a(q-R_d)-(q\Gamma+KR_d)]}{[C_a+K-\lambda a(w_{sat}-w_a)]\lambda a(w_{sat}-w_a)}}\right.$$
$$\left.[C_a+K-2\lambda a(w_{sat}-w_a)].\ \ +(q-R_d)\ C_a-(q\Gamma+KR_d)-q\ (K+\Gamma)\right] \quad (14)$$

Once g is known, the Lagrangian multiplier λ can—in principle—be calculated by performing the integration in the second equation in (8) explicitly. It can be shown (Konrad et al., 2008) that λ is closely connected to soil water availability and measures the 'cost of water' for the plant: high λ indicates shortcoming, low λ indicates abundance of soil water. Notice that in parts of the literature the Lagrangian multiplier is designated by the reciprocal of λ as used here; then, the interpretation of λ should be reversed.

The desired atmospheric CO_2 concentration C_a under which the fossilised leaf has grown is found by inserting expression (12) into expression (4), resulting in a relation $\nu(C_a)$. The solution of this equation for C_a is straightforward, albeit a bit tedious.

2.1.2 | Reduced order model and the model of Franks et al.

In terms of their physical basis and their mathematical structure these two models are similar, although they appear to be quite different, at first sight. The apparent dissimilitude is due to a different notation and various approximations that do not affect the mathematical core and reasoning.

Reduced order model

In this model, the combination of Equations (1), (2) and (5) produces (Konrad et al., 2017):

$$g = \frac{q(\kappa C_a-\Gamma)}{(1-\kappa)C_a(\kappa C_a+K)}-\frac{R_d}{(1-\kappa)C_a}, \quad (15)$$

the right-hand side of which contains—apart from the photosynthesis parameters and κ—only C_a. Insertion of (15) into (2) and (3) yields:

$$A = q\ \frac{\kappa C_a-\Gamma}{\kappa C_a+K}-R_d, \quad (16)$$

$$E = \frac{q(\kappa C_a-\Gamma)-R_d(\kappa C_a+K)}{(1-\kappa)C_a(\kappa C_a+K)}\ a(w_{sat}-w_a), \quad (17)$$

Similarly as in Section 2.1.1, combining expressions (4) and (15) results in an expression $\nu(C_a)$ that is quadratic in C_a and can be solved for the atmospheric CO_2 concentration C_a under which the fossilised leaf had grown.

The model of Franks et al.

The model of Franks et al. (2014) is also based on Equations (1), (2), (4) and (5):

- Equation (1) in Franks et al. (2014) is equivalent to Equation (2) of Section 1.2; notice that although they do not assign an extra variable to the ratio C_i/C_a (such as $\kappa = C_i/C_a$ we have introduced as Equation (5)) they treat C_i/C_a as an independent quantity.
- Equations (2) and (3) in Franks et al. (2014) are equivalent to (4).
- Equation (6) in Franks et al. (2014) can be derived from the photosynthesis model (1) when the following assumptions are made:
  1. neglecting the quantity R_d,
  2. assuming that photosynthesis is RuBP rather than Rubisco-limited, implying $K = 2\Gamma$,
  3. dividing the expression $A = q(C_i - \Gamma)/(C_i + 2\Gamma)$ resulting from (1) by an assimilation rate $A_0 = q(C_{i,0} - \Gamma)/(C_{i,0} + 2\Gamma)$ related to a different CO_2-level $C_{i,0}$ and
  4. replacing $C_i = \kappa C_a$ and $C_{i,0} = \kappa_0 C_{a,0}$ [due to (5), see Kowalczyk et al. (2018)]

$$A = A_0\ \frac{(\kappa C_a-\Gamma)\ (\kappa_0 C_{a,0}+2\Gamma)}{(\kappa C_a+2\Gamma)\ (\kappa_0 C_{a,0}-\Gamma)}. \quad (18)$$

The two Equations (1) and (6) of Franks et al. (2014) contain the two unknowns C_a and A for which they can be solved, either iteratively [as proposed in Franks et al. (2014)], or directly: Insertion of their relation (1) into (6) produces a quadratic equation for C_a. The solution of this equation is tedious but otherwise straightforward. [Notice that expression (18) makes $q \equiv V_{c,\max}$ vanish from the system of equations; the information stored in $V_{c,max}$ is now obtained from the values A_0 and $C_{a,0}$ of a (preferably closely related) plant growing under current conditions.]

2.1.3 | The simplified reduced order model

The 'simplified model' (Konrad et al., 2017) emerges from the reduced order model of Section 2.1.2 in the limit $\Gamma \to 0$ and $R_d \to 0$, or, more precisely, if C_i (or C_a, in view of the relation $C_i = \kappa C_a$) is high enough and the following conditions apply:

$$C_a \gg \frac{\Gamma}{\kappa}, \quad (19)$$

$$C_a \gg \frac{q\Gamma+KR_d}{\kappa(q-R_d)}. \quad (20)$$

Notice that (20) is more restrictive than (19), provided $R_d < q$, which is the case for real plants.

Neglecting Γ, the CO_2 compensation point, and R_d, the mitochondrial respiration rate, simplifies the structure of the assimilation model (1) to $A = qC_i/(C_i + K)$, hereby reducing its accuracy for small C_i (with respect to C_a). However, these simplifications remain plausible at high C_i and the mathematical structures of the two assimilation models remain similar (i.e., nocturnal and mitochondrial respiration are no

longer part of the model, but the asymptotic behaviour for high C_i is still present). Thus, the deviations of the simple from the full assimilation model (1) can be tolerated for high enough values of atmospheric CO_2.

In the limits $\Gamma \to 0$ and $R_d \to 0$ of the approximations (20), the relation between stomatal density ν and C_a of the reduced order model simplifies to:

$$\nu = \frac{\left[\frac{q}{(1-\kappa)D_{CO_2}}\frac{d_{st}}{a_{st}}\right]}{C_a - \left[\frac{q\beta}{(1-\kappa)D_{CO_2}} - \frac{K}{\kappa}\right]}, \tag{21}$$

where $\beta := d_{bl} + d_{as}\,\frac{\tau_{as}^2}{n_{as}}$.

2.2 | Phenomenological approaches

The stomatal ratio model comes in two varieties: stomatal ratio can mean the ratio of stomatal densities or the ratio of stomatal indices that are defined in terms of the densities of stomatal and epidermal cells.

2.2.1 | Stomatal ratio model (based on stomatal density)

The starting point of the model variety based on stomatal density (McElwain & Chaloner, 1995, 1996) is the observation that the ratio of the stomatal densities ν of two plants (e.g., a fossil one, ν, and an extant one, ν_{ext}, of the same species) is roughly reciprocally proportional to the ratio of the atmospheric carbon dioxide concentrations wherein these plants lived (Kleidon, 2007; Wynn, 2003), that is,

$$\frac{\nu_{\text{ext}}}{\nu} = \frac{C_a}{C_{a,\text{ext}}}. \tag{22}$$

This statement is equivalent to

$$\nu = \frac{k_{\text{SD}}}{C_a}, \tag{23}$$

where ν_{ext} and $C_{a,\,\text{ext}}$ have been amalgamated into the constant

$$k_{\text{SD}} = \nu_{\text{ext}}\, C_{a,\text{ext}} \tag{24}$$

Therefore, knowledge of a single known data pair (ν_{ext}, $C_{a,\text{ext}}$) is sufficient to derive palaeo-CO_2 via relation (23). If stomatal density ν depends on atmospheric CO_2 but is largely unaffected by all other environmental conditions, such as atmospheric humidity or air temperature, the parameter k_{SD} should have one constant value for all individuals of the same species. Notice, that relation (22) implies that, in a (ν, C_a)-diagram, all (ν, C_a)-pairs of a given species should lie on the curve defined by expression (23).

2.2.2 | Stomatal ratio model (based on stomatal index)

In the stomatal index model, stomatal density in Equation (23) is replaced by the stomatal index:

$$\text{SI} = \frac{\nu}{\nu + \epsilon} \times 100. \tag{25}$$

Here, ϵ denotes the number of epidermal cells per leaf area and ν is the number of stomata per leaf area; therefore, $\nu/(\nu + \epsilon)$ represents the fraction of cells of the leaf surface that are equipped with stomata and SI denotes the related percentage. In this context, it is advantageous to use the quantity σ (Sack & Buckley, 2016), defined by:

$$\sigma = \frac{\text{SI}}{100} = \frac{\nu}{\nu + \epsilon} = \frac{1}{1 + (\epsilon/\nu)}. \tag{26}$$

The rightmost version of this equation indicates that σ depends solely on the ratio of ϵ and ν. Following the same reasoning that led from (22) to (23) we obtain in a first step:

$$\frac{\sigma_{\text{ext}}}{\sigma} = \frac{C_a}{C_{a,\text{ext}}} \tag{27}$$

Introducing the constant:

$$k_{\text{SI}} = \sigma_{\text{ext}}\, C_{a,\text{ext}}, \tag{28}$$

this can be rewritten:

$$\sigma = \frac{k_{\text{SI}}}{C_a}, \tag{29}$$

or, equivalently,

$$C_a = \frac{k_{\text{SI}}}{\sigma} = k_{\text{SI}}\left(1 + \frac{\epsilon}{\nu}\right) \tag{30}$$

The last version results with the help of relation (26). This is the sought-after model for determining C_a from σ (respective ν and ϵ). When applying this method, it is tacitly assumed that physiological changes that occurred between past plants and their present representatives can be ignored, as well as the effects of environmental parameters other than C_a.

2.2.3 | Transfer functions ('full calibration models')

Another widely used approach to reconstruct palaeo-CO_2 on the basis of empirical data utilises fitting of a number of observed (ν, C_a) data pairs by using an appropriate fitting function (Barclay & Wing, 2016; Beerling & Royer, 2002; García-Amorena, Wagner, van Hoof, & Manzaneque, 2006; Hincke, Broere, Kürschner, Donders, & Wagner-Cremer, 2016; Kürschner, Kvacek, & Dilcher, 2008; Kürschner, Wagner, Visscher, & Visscher, 1997).

The basic idea is as follows: (a) measurements of ν, ϵ and C_a-values from a number of individuals of an extant species, which is

considered to be a suitable relative of the considered fossil taxon, grown under different atmospheric CO_2 concentrations yield a cloud of (ν, C_a)- or (σ, C_a)-pairs; (b) linear or non-linear regressions methods allow fitting of these data points to a (ν, C_a)- or (σ, C_a)-curve which can then be used (c) to infer palaeo-CO_2 from stomatal density or stomatal index of fossil leaves.

Also, this method rests on the tacit assumption that physiological, environmental or climatic changes that occurred between fossil plants and their present representatives can be ignored. Since it is difficult to maintain very low or very high C_a-values over a long time period (e.g., in a greenhouse), transfer curves obtained from measurements of ν and ϵ under medium C_a-values are often extrapolated into these regions. In view of possible saturation or depletion phenomena that are connected with photosynthesis and may occur especially at very low or very high C_a-values this practise is problematic.

2.2.4 | The model of Schubert and Jahren

Denoting the ratios of the stable carbon isotopes ^{12}C and ^{13}C in the atmosphere and in the plant tissue by $\left(\frac{^{13}C}{^{12}C}\right)_{CO_2}$ and $\left(\frac{^{13}C}{^{12}C}\right)_p$, respectively, the positive discrimination of CO_2 molecules consisting of the lighter isotope by diffusion along the pathway through the plant leaf and the subsequent assimilation machinery can be expressed as:

$$\Delta^{13}C_p = \frac{\left(\frac{C}{^{12}C}\right)_{CO_2} - \left(\frac{^{13}C}{^{12}C}\right)_p}{\left(\frac{^{13}C}{^{12}C}\right)_p} = \frac{\delta^{13}C_{CO_2} - \delta^{13}C_p}{1 + \delta^{13}C_p}. \quad (31)$$

The second version results if the relation $\delta^{13}C_{sample} = \left[\left(\frac{^{13}C}{^{12}C}\right)_{sample} / \left(\frac{^{13}C}{^{12}C}\right)_{standard}\right] - 1$ is used; the subscript 'sample' represents CO_2 or p (=plant).

Schubert and Jahren (2012) inferred from systematic measurements of $\Delta^{13}C$ in which they kept all environmental parameters constant, apart from atmospheric CO_2 concentration, that the relation:

$$\Delta^{13}C = \frac{\Delta^{13}C_{max}\ m\ (C_a - f)}{\Delta^{13}C_{max} + m(C_a - f)}, \quad (32)$$

acceptably fits these measurements provided the parameters m, f and $\Delta^{13}C_{max}$ are assigned suitable values. This relationship was found to hold in further work by Cui and Schubert (2016, 2018). Hence, relation (32) represents a calibration curve that can be used to reconstruct palaeo-CO_2 from the $\Delta^{13}C$ value of fossil plant material by solving (32) for:

$$C_a = \frac{\Delta^{13}C_{max}(fm + \Delta^{13}C) - fm\ \Delta^{13}C}{m(\Delta^{13}C_{max} - \Delta^{13}C)}. \quad (33)$$

3 | STRUCTURAL DIFFERENCES BETWEEN THE MODELS

In the following, models derived explicitly from established physical principles and physiological processes will be compared to phenomenological models based on assumptions and data-fitting procedures (cf. Figure 1). The pragmatic way to decide whether any of the different approaches are in a given context superior or equal (with respect to accuracy of predictions) to their competitors would be to apply all models to extant plants and to assume that the results are transferable to their fossil counterparts, because the ultimate measure for the quality of any model is usually its capability to provide predictions which are consistent with results of independent measurements. In the case of proxy approaches for paleoenvironments, this is, however, quite difficult, because this kind of 'test' refers to extant data sets which are to a greater or lesser extent source of the various methods.

In what follows, another path will be taken by exploiting the fact that phenomenological models are in fact also based on basic principles of physics and physiology, even if they are not explicitly derived from these principles. To this end, we compare the functional form of a phenomenological and a mechanistic model and examine if one model can be brought into agreement with the other one by the application of reasonable approximations and/or additional assumptions. However, it must be emphasised that unique interpretations of phenomenological parameters in terms of mechanistic quantities may be impossible. Different mechanistic models do necessarily produce different expressions for these parameters.

In this section, we shall proceed as follows. First, an inquiry into the two groups of mechanistic models is conducted so as to establish a ranking with respect to complexity and comprehensiveness. To extend this ranking to phenomenological models, we examine them as outlined above. Afterwards, we will be able to discuss the structural differences of the models.

3.1 | Complexity and comprehensiveness of the mechanistic models

The structure of mechanistic models presented in Section 2 suggests a certain hierarchy in terms of their complexity:

- In the reduced order model and in the model of Franks et al., expression (15) for leaf conductance g depends merely on atmospheric CO_2 concentration C_a, the ratio $\kappa = C_i/C_a$ between leaf internal and atmospheric CO_2 concentration and the photosynthesis parameters q, K, Γ, R_d. The latter introduce also a dependence on temperature T. In these models leaf conductance g is constrained exclusively by the relations (1), (2) and (5), representing the assimilation machinery and the carbon dioxide exchange between leaf and atmosphere; transpiration is a mere consequence of this, as implied by (3) (i.e., water uptake is entirely dictated by

the carbon demands of the plant): Water related quantities, such as atmospheric humidity w_a or soil water availability are not accounted for.

- This restriction applies also to the 'simplified model' of Konrad et al. (2017) (see Section 2.1.2) whose only difference to the reduced order model is that it employs a simpler photosynthesis model, namely the limit $\Gamma \to 0$ and $R_d \to 0$ of the Farquhar model (see (1)).
- In the optimisation Equations (9) and (11), however, transpiration appears on an equal footing with assimilation; hence, the resulting expression (12) for leaf conductance g includes the water related quantities cited above.

In this sense, the optimisation models are more comprehensive than the reduced order model, the model of Franks et al. (2014) and the 'simplified model' of Konrad et al. (2017). Figure 2 summarises the structural complexity of the models considered here.

3.2 | Mechanistic interpretation of phenomenological models

3.2.1 | Stomatal ratio model (based on stomatal density)

To shed some light on the meaning of the parameter k_{SD}, we compare the expressions relating C_a to ν in the mechanistic simplified reduced order model (expression (21)) to the density-based stomatal ratio model (expression (23)). We then ask whether there are reasonable approximations to reduce expression (21) of the mechanistic model to the functional form (23) of the phenomenological model. If so, it is possible to interprete the model parameter k_{SD} in terms of mechanistic quantities that can be independently measured or inferred.

Comparing the right-hand sides of (21) and (23) with regard to their C_a dependencies one finds that they can be reconciled by demanding that the denominator of the right-hand side of (21) is dominated by C_a, that is:

$$C_a \gg \left| \frac{q}{(1-\kappa)D_{CO_2}} \left(d_{bl} + d_{as} \frac{{\tau_{as}}^2}{n_{as}} \right) - \frac{K}{\kappa} \right|, \tag{34}$$

Then, the parameter k_{SD} in (23) can be identified with the numerator on the right-hand side of (21), that is,

$$k_{SD} = \frac{q}{(1-\kappa)D_{CO_2}} \frac{d_{st}}{a_{st}}. \tag{35}$$

The problem is, that Equation (34) compares (on its right-hand side) morphological quantities from fossilised leaves and photosynthetic parameters obtained from nearest living relatives with the quantity C_a (on its left-hand side) which is not yet known. The remedy is to apply relation (23) to eliminate C_a in favour of ν resulting in an inequality relating similar quantities:

$$\nu \ll \frac{\frac{d_{st}}{a_{st}}}{\left| d_{bl} + d_{as} \frac{{\tau_{as}}^2}{n_{as}} - \frac{D_{CO_2}(1-\kappa)K}{\kappa\, q} \right|}. \tag{36}$$

In any case, if (36) is valid the application of the density-based stomatal ratio model (expression (23)) to a fossil leaf exhibiting stomatal density ν is justified, and the parameter k_{SD} in (23) can be identified with the numerator of the right-hand side of (21), that is, it is given by (35). Notice that:

- D_{CO_2}, q and K depend on temperature [for the explicit functional form consult Nobel (2005) and Bernacchi et al. (2003)], and
- if (36) is valid for a given stomatal density ν it is also valid for all stomatal densities smaller than this ν. That is, condition (36) defines an interval 0…ν, and—via (23)—an interval C_a…∞ wherein the use of (23) is legitimate.

What does that mean in practise? Note that the 'much smaller' sign ('≪') in (36) means a certain leeway for deciding what is 'small enough'. Ignoring this arbitrariness can introduce considerable error with respect to CO_2 reconstruction. We can demonstrate this by using values for *Ginkgo biloba* from Table 1 (for T = 20°C). Upon

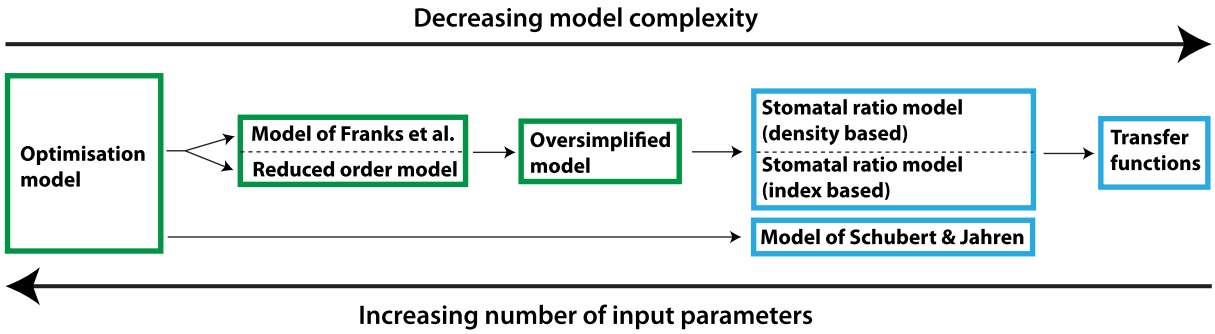

FIGURE 2 Hierarchy of the models discussed here implied by the differences in their structural complexity. Mechanistic models are indicated by a green frame and phenomenological models are indicated by a blue frame. Increased model complexity comes at a cost: a more detailed (and hopefully more accurate) output requires a more detailed knowledge of input parameters [Color figure can be viewed at wileyonlinelibrary.com]

TABLE 1 Model parameters related to *G. biloba* together with their dimensions

Quantity (units)	Explanation	Numeric value
Environmental parameters		
T (°C)	Temperature (air)	Varied
w_{rel} (–)	Relative atmospheric humidity	Varied
w_a (mol/m^3)	Leaf external humidity, $w_a = w_{rel}w_{sat}$	Calculated
w_l (–)	Relative leaf internal humidity (≈saturation value)	≈1
w_{sat} (mol/m^3)	Saturation value of humidity (depends on T)	Calculated
λ (–)	'Cost of water' (Lagrange multiplier of optimisation model)	0.0026
κ (–)	$\kappa = C_i/C_a$, reduced order model	0.71
κ (–)	$\kappa = C_i/C_a$, simplified reduced order model	0.65
$\tilde{a}$ (–)	Isotopic fractionation due to diffusion through the plant leaf	4.4×10^{-3}
$\tilde{b}$ (–)	Isotopic fractionation due to catalysis by Rubisco	27×10^{-3}
D_{CO_2} (m^2/s)	Diffusion constant of CO_2 at T = 25°C (depends on T)	1.55×10^{-5}
D_{H_2O} (m^2/s)	Diffusion constant of water vapour at T = 25°C (depends on T)	2.49×10^{-5}
a (–)	$a = D_{H_2O}/D_{CO_2}$	1.6
k_{SD} (1/mm^2)	Constant in density-based stomatal ratio model (see (24))	0.034
k_{SI} [–]	Constant in index-based stomatal ratio model (see (28))	28.7×10^{-6}
Biochemical parameters from *G. biloba*		
q (μmol/m^2/s)	Carboxylation limited by Rubisco or RuBP at T = 25°C[a]	7.3
K (μmol/m^3)	Contains Michaelis–Menten constants[a]	13,925
Γ (μmol/m^3)	CO_2 compensation point[a]	2,408
R_d (μmol/m^2/s)	Mitochondrial respiration rate[a]	0.16
Leaf anatomical parameters from *G. biloba*		
ν (1/mm^2)	Stomatal density[b]	85
ϵ (1/mm^2)	Density of epidermal cells[b]	1,100
σ (–)	$\sigma = \nu/(\nu + \epsilon)$	0.071
SI (–)	Stomatal index, SI = 100 σ	7.1
a_{st} (μm^2)	Stomatal pore area[b,c]	12.3
d_{st} (μm)	Depth of stomatal pore[b]	33.8
d_{as} (μm)	Thickness of assimilating tissue[b]	217.7
τ_{as} (–)	Tortuosity of assimilating tissue[b]	1.571
n_{as} (–)	Porosity of assimilating tissue[b]	0.35
d_{bl} (mm)	Thickness of boundary layer[d]	0.66
l_c (mm)	Characteristic leaf length[b]	84

Note: Specific values of parameters designated as 'varied' are given in the figure captions.
[a]For a list of the data sources for the biochemical demand parameters, see Konrad et al., 2008.
[b]Values determined from the literature (see also Konrad et al., 2008).
[c]Stomatal pore area is calculated as elliptic shape.
[d]Leaf boundary layer thickness calculated for 1.0 m/s as a typical wind velocity (Nobel, 2005).

insertion of these values into the right-hand side of (36), it follows $\nu \lesssim 294/mm^2$. If we decide that 'small enough' requires a 10-fold smaller value (i.e., one order of magnitude), we arrive at the condition that stomatal density should be not larger than $\nu \gtrsim 30/mm^2$ when the density-based stomatal ratio method is to be used. In Table 1, however, ν amounts to $85/mm^2$, and the stomatal ratio method should not be used.

Equivalently, the problem can also be approached via relation (34) which provides a lower bound for CO_2: here, the values of Table 1 result in $C_a \gg 242$ μmol/mol. If we interpret '$\gg$' as requiring C_a to be

10-fold higher for applying the stomatal ratio method, then we arrive at a minimum level of $C_a \gtrsim 2420$ μmol/mol. However, the factor 10 used above (equivalent to one order of magnitude) is by no means unique; its choice should be reasonable but depends always on circumstances; depending on the ultimate purpose of the reconstruction, even two orders of magnitude may be adequate to arrive at feasible results.

3.2.2 | Stomatal ratio model (based on stomatal index)

In the case of the index-based stomatal ratio model, we proceed in close analogy. We first transform expression (21) by means of (26) to:

$$\sigma = \frac{\left[\frac{q}{(1-\kappa)D_{CO_2}}\frac{d_{st}}{\epsilon a_{st}}\right]}{C_a - \left\{\frac{q}{(1-\kappa)D_{CO_2}}\left(d_{bl} + d_{as}\,\frac{\tau_{as}{}^2}{n_{as}} - \frac{d_{st}}{\epsilon a_{st}}\right) - \frac{K}{\kappa}\right\}}. \tag{37}$$

As above we can now require that the absolute value of the term in braces in the denominator strictly vanishes. Or we require merely that this term is much smaller than C_a, yielding:

$$C_a \gg \left|\frac{q}{(1-\kappa)D_{CO_2}}\left(d_{bl} + d_{as}\,\frac{\tau_{as}{}^2}{n_{as}} - \frac{d_{st}}{\epsilon a_{st}}\right) - \frac{K}{\kappa}\right|. \tag{38}$$

Using (29), this condition can be rewritten as a condition for σ,

$$\sigma \ll \frac{\frac{d_{st}}{\epsilon a_{st}}}{\left|d_{bl} + d_{as}\,\frac{\tau_{as}{}^2}{n_{as}} - \frac{d_{st}}{\epsilon a_{st}} - \frac{D_{CO_2}(1-\kappa)K}{\kappa\, q}\right|}. \tag{39}$$

The parameter k_{SI} in (29) adopts—on comparison with (37)—a slightly different value than its counterpart (35), namely:

$$k_{SI} = \frac{q}{(1-\kappa)D_{CO_2}}\frac{d_{st}}{\epsilon a_{st}}. \tag{40}$$

3.2.3 | Transfer functions

The transfer function method relies on preformulated and arbitrarily selected equations used for fitting measured data, and therefore bears no direct link to mechanistic concepts. In principle, it would be possible to connect (and in a sense to 'explain') one or more of the indeterminate parameters of the used fitting curves with parameters occurring in one of the mechanistic models of Section 2.1, similarly as we proceeded in Sections 3.2.1 and 3.2.2 in the case of the stomatal ratio models. However, a variety of equations are used for fitting, among them sigmoidal shaped solutions of the logistic equation (Kürschner et al., 1997) and power-curve regressions (Barclay & Wing, 2016). Further examples can be found in Beerling and Royer (2002) and Wynn (2003). Since fitting curves are selected with respect to the quality of the curve fit only and therefore depending on the shape of the individual scatterplot, it appears to be not possible to identify a special 'function skeleton' structurally homologous with one of the mechanistic approaches.

3.2.4 | The model of Schubert and Jahren

To date no derivations of expression (32) from general principles appeared in the literature known to the authors although the mechanism behind this equation is, at least for C_3-plants, well known (Schubert & Jahren, 2012) and has been described some time ago by Farquhar et al. (1982). Isotopic fractionation due to diffusion and assimilation obeys the relation:

$$\Delta^{13}C = \tilde{a} + \left(\tilde{b} - \tilde{a}\right)\frac{C_i}{C_a}, \tag{41}$$

where $\tilde{a}$ is the isotopic fractionation due to diffusion into the leaf and $\tilde{b}$ is the fractionation occurring during carboxylation (Farquhar et al., 1982). Taking (41) as a starting point, such a derivation can be performed by employing the optimisation model discussed in Section 2.1 to express C_i in terms of C_a and the photosynthetic and environmental parameters. This is achieved by inserting expression (13) for the assimilation rate into the assimilation model (1) and solving for C_i. Utilizing the result in (41) yields the mechanistic counterpart of (32):

$$\Delta^{13}C_{mech} = \tilde{a} + \left(\tilde{b} - \tilde{a}\right)\left(\frac{C_a(q\Gamma + KR_d) - K\lambda a(w_{sat} - w_a)\sqrt{\frac{q\,(K+\Gamma)[C_a(q-R_d) - (q\Gamma + KR_d)]}{[C_a + K - \lambda a(w_{sat} - w_a)]\lambda a(w_{sat} - w_a)}}}{C_a\left[q(\Gamma + K) - \lambda a(w_{sat} - w_a)\sqrt{\frac{q\,(K+\Gamma)[C_a(q-R_d) - (q\Gamma + KR_d)]}{[C_a + K - \lambda a(w_{sat} - w_a)]\lambda a(w_{sat} - w_a)}}\right]}\right). \tag{42}$$

As in Sections 3.2.1 and 3.2.2, parameters m, f and $\Delta^{13}C_{max}$ of the phenomenological relation (32) can be expressed in terms of quantities appearing in the mechanistic relation (42). The following properties of $\Delta^{13}C$, as defined in relation (32), are used:

$$\lim_{C_a \to \infty} \Delta^{13}C = \Delta^{13}C_{max}, \tag{43}$$

$$\Delta^{13}C\big|_{C_a = f} = 0, \tag{44}$$

$$\left.\frac{d\Delta^{13}C}{dC_a}\right|_{C_a = f} = m. \tag{45}$$

Applying these relations to $\Delta^{13}C_{mech}$, as defined in relation (42), and setting $R_d = 0$ and $\Gamma = 0$ (these two variables are not overly influential and neglecting them avoids overlong expressions) one obtains:

$$\Delta^{13}C_{max} = \frac{\sqrt{K\lambda a(w_{sat}-w_a)}\left(\tilde{a}-\tilde{b}\right)+\tilde{b}K-\tilde{a}\lambda a(w_{sat}-w_a)}{K-\lambda a(w_{sat}-w_a)}$$
$$f = \frac{K\lambda a(w_{sat}-w_a)\left(\tilde{b}-\tilde{a}\right)^2}{\tilde{b}^2K-\tilde{a}^2\lambda a(w_{sat}-w_a)} \qquad (46)$$
$$m = \frac{\left(\tilde{b}^2K-\tilde{a}^2\lambda a(w_{sat}-w_a)\right)^2}{2K\lambda a(w_{sat}-w_a)\left[\tilde{b}K-\tilde{a}\lambda a(w_{sat}-w_a)\right]\left(\tilde{b}-\tilde{a}\right)^2}.$$

Calculating $\Delta^{13}C_{max}$, f and m in this way effectuates that the functions $\Delta^{13}C(C_a)$ (see (32)) and $\Delta^{13}C_{mech}(C_a)$ share the zero at $C_a = f$, the slope m at the common zero and the asymptotic behaviour for $C_a \to \infty$.

Notice that the right-hand sides of (46) vary with T, w_{rel} and λ. Since $\tilde{a}$ and $\tilde{b}$ in (41) are constants this implies that the ratio C_i/C_a must also vary with temperature and plant water conditions (i.e., humidity and 'cost of water' λ).

4 | DISCUSSION: APPLICABILITY AND LIMITS OF THE MODELS

4.1 | Comparison of the models

Figures 3 and 4 show (SI, C_a)-curves resulting from the different models obtained with the data of Table 1 (with the exception of the model of Schubert and Jahren which uses neither stomatal density nor index). To make the model results comparable, they are all expressed—if necessary by applying relation (25)—in the form $SI = f(C_a)$. For the atmospheric temperature $T = 20^\circ$C and the relative atmospheric humidity $w_{rel} = 0.75$ all curves intersect at the point ($C_{a,ext}$, SI_{ext}) = (400 μmol/mol, 7.2), marked by a black dot, and typical for extant *G. biloba* trees.

As is justified by its unmatched complexity in the model hierarchy depicted in Figure 2, we use the optimisation model of Section 2.1 as a benchmark for the accuracy of the other models. A first glance at Figures 3 and 4 corroborates the notion that complexity is the price of accuracy: the distance of model curves from the benchmark curve (solid, red) increases with decreasing model complexity.

4.1.1 | Influence of climate

The subfigures of Figure 3 represent variations of both temperature and humidity, T = (15°C, 20°C, 25°C) and w_{rel} = (0.5, 0.75, 0.9). Only the optimisation model and both reduced order models include environmental parameters, with the optimisation model requiring temperature, air humidity and soil water conditions (hidden in the parameter λ), while both the reduced order model and the simplified reduced order model require only temperature. The stomatal ratio models include neither temperature nor humidity. These structural differences between models with respect to considering climate contribute largely to the different model results.

Figures 3 and 4 convey the overall impression that when CO_2 exceeds about 300 μmol/mol, model curves at low temperatures and humidities are much closer to one another than at high temperatures and humidities.

If one accepts the optimisation model as benchmark, the stomatal ratio models underestimate C_a for all climatic conditions; the effect is particularly grave under conditions of high humidity and/or under high temperature (Figure 3c,f–i). At moderate and high humidities (Figure 3d–i) the reduced order and simplified models also underestimate CO_2 but to a lesser extent than the non-mechanistic models. This can be attributed to the fact that the mechanistic models react on temperature, the stomatal ratio models, however, do not. For low humidity and beyond $C_a \gtrsim 1000$ μmol/mol the mechanistic models are quite close together.

The diagrams in Figure 4 corroborate these structural differences. They illustrate the deviations $\Delta SI_{model} = SI_{model} - SI_{opt}$ of all models from the optimisation model. *Opt* denotes the optimisation model and *model* denotes either of the models depicted in Figure 3; setting *model* = *opt* produces the red base line.

For most temperature and humidity combinations, the non-optimisation models tend to underpredict CO_2; indeed, the simpler the model, the greater the underprediction (Figures 3 and 4). It is common for stomatal ratio-based and transfer function-based CO_2 estimates for the Paleogene to be anomalously low [e.g., Barclay and Wing (2016); Kowalczyk et al. (2018); see also compilations by Beerling and Royer (2011); Foster et al. (2017)]. The structural limitations of these simpler approaches identified here may explain their persistent underprediction.

4.1.2 | Influence of atmospheric CO_2 concentration

Figures 3 and 4 suggest that all curves in all subfigures converge for high C_a, irrespective of the values of T and w_{rel}. This can be understood from the structure of the mechanistic models: if one brings them into the form $\sigma = f(C_a)$ and expands the results in power series with respect to $1/C_a$, one finds that for $C_a \to \infty$ they are dominated by a term k/C_a (with k = const.), that is, $\sigma \approx k/C_a$ for $C_a \to \infty$. Structurally, this is equivalent to $\sigma = k_{SI}/C_a$, the basic Equation (29) of the stomatal ratio models. For high enough C_a even a difference between k and k_{SI} becomes insignificant. It is therefore not surprising that the stomatal ratio models, indicated by the magenta and violet lines in Figure 3, approach their mechanistic counterparts (red, green and blue) for high enough C_a. Ultimately, for *very* high C_a, all model curves approach asymptotically the value SI = 0.

It should be noted, however, that the merely asymptotic convergence of the models for $C_a \to \infty$ means that the less complex models are only applicable for high C_a-regimes. Moreover, the convergence behaviour depends on climate. Especially for warm and humid climates (cf. Figure 3h,i), a minimum C_a of several 1,000 μmol/mol is required, limiting the practical applicability of simple models severely.

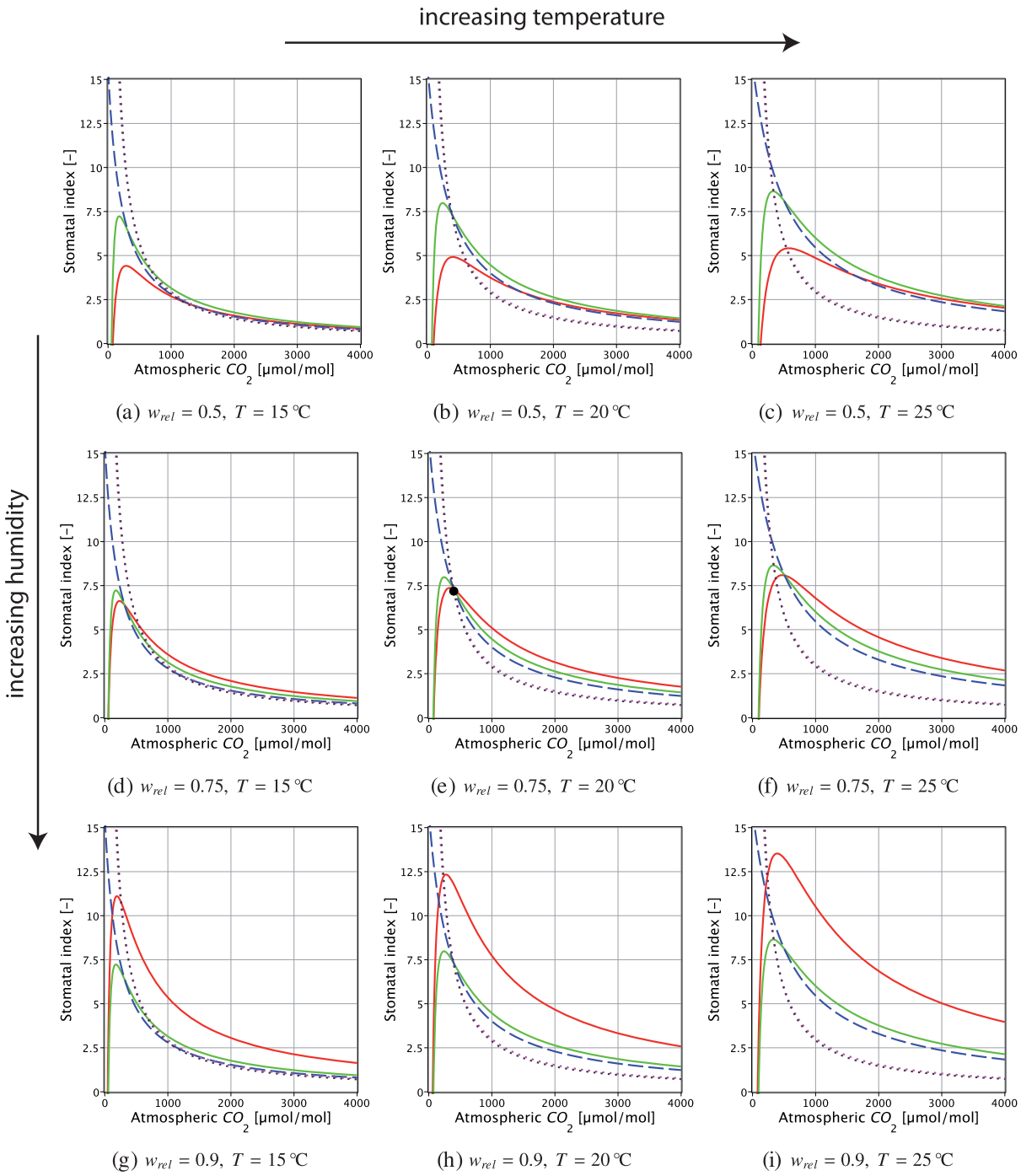

FIGURE 3 Stomatal indices of *G. biloba* as a function of atmospheric C_a. The curves are calculated via the optimisation model (solid red lines), the reduced order model (solid green lines), the simplified model (broken blue lines), the density-based stomatal ratio model (dotted magenta lines) and the index-based stomatal ratio model (dotted violet lines). The black dot in subfigure (e) marks the point ($C_{a,\mathrm{ext}}$, SI_{ext}) = (400 μmol/mol, 7.2), typical for extant *G. biloba* trees. Values of air humidity and air temperature used for calculating the curves are as indicated in the subfigures. Notice that the optimisation model depends on humidity *and* temperature, the reduced order model and the simplified reduced order model depend *only* on temperature and the stomatal ratio models depend neither on humidity nor on temperature. Other input values are given in Table 1 [Color figure can be viewed at wileyonlinelibrary.com]

4.1.3 | The model of Schubert and Jahren

Since the model of Schubert and Jahren is based on a completely different approach, a direct comparison with the other models is not possible; the disparity of the model approaches, or, more precisely, the absence of leaf anatomical quantities precludes calculating stomatal index from the model of Schubert and Jahren. It is therefore difficult to locate its definite position within the ranking order defined by the other models (cf. Figure 2). Lacking any reference to temperature, humidity, soil water content or leaf anatomy it is, in any case, less

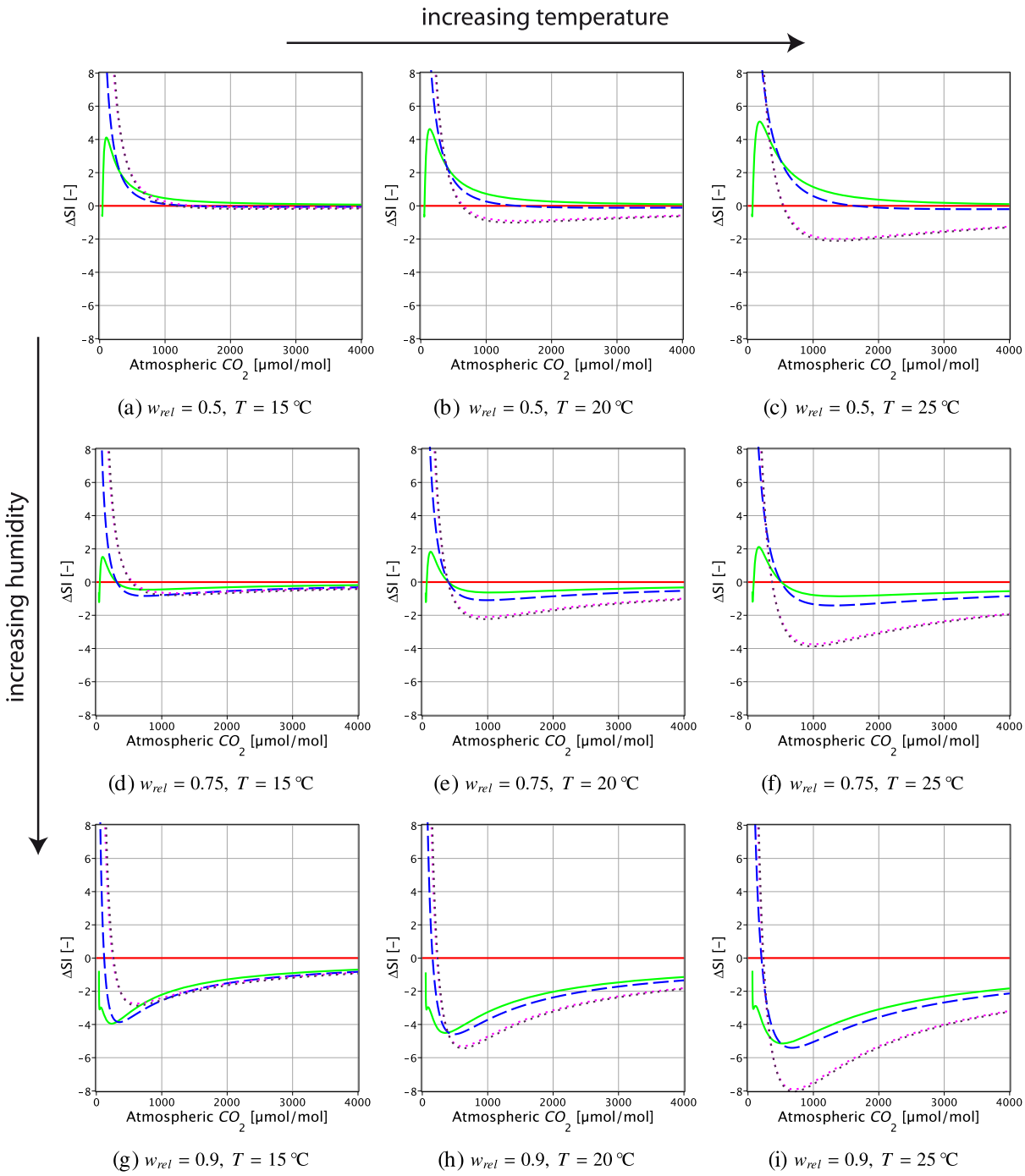

FIGURE 4 Deviations of stomatal indices from SI_{opt} as a function of atmospheric C_a. The deviations $\Delta SI_{model} = SI_{model} - SI_{opt}$ are relative to the optimisation model (*opt*) for *G. biloba* which serves as benchmark. *Model* denotes either of the following models (cf. also Figure 3): Optimisation model (solid red lines), reduced order model (solid green lines), simplified reduced order model (broken blue lines), density-based stomatal ratio model (dotted magenta lines) and index-based stomatal ratio model (dotted violet lines). Values of air humidity and air temperature used for calculating the red, green and blue lines are indicated. Other input values are given in Table 1 [Color figure can be viewed at wileyonlinelibrary.com]

complex than the optimisation model, from which it can be derived, according to Section 3.2.4.

The diagrams in Figure 5 compare the discrimination $\Delta^{13}C$ calculated via the model of Schubert and Jahren, if interpreted in terms of the optimisation model (dashed, blue curves), with the optimisation model combined with relation (41).

The two curves nearly coincide in Figure 5e but diverge in the subfigures related to the other variations of temperature and atmospheric humidity. This is because the optimisation model, from which $\Delta^{13}C_{mech}$ is derived, depends not alone on the value of the atmospheric CO_2-concentration C_a but, according to (42), also on the environmental variables air temperature T, atmospheric humidity w_a and

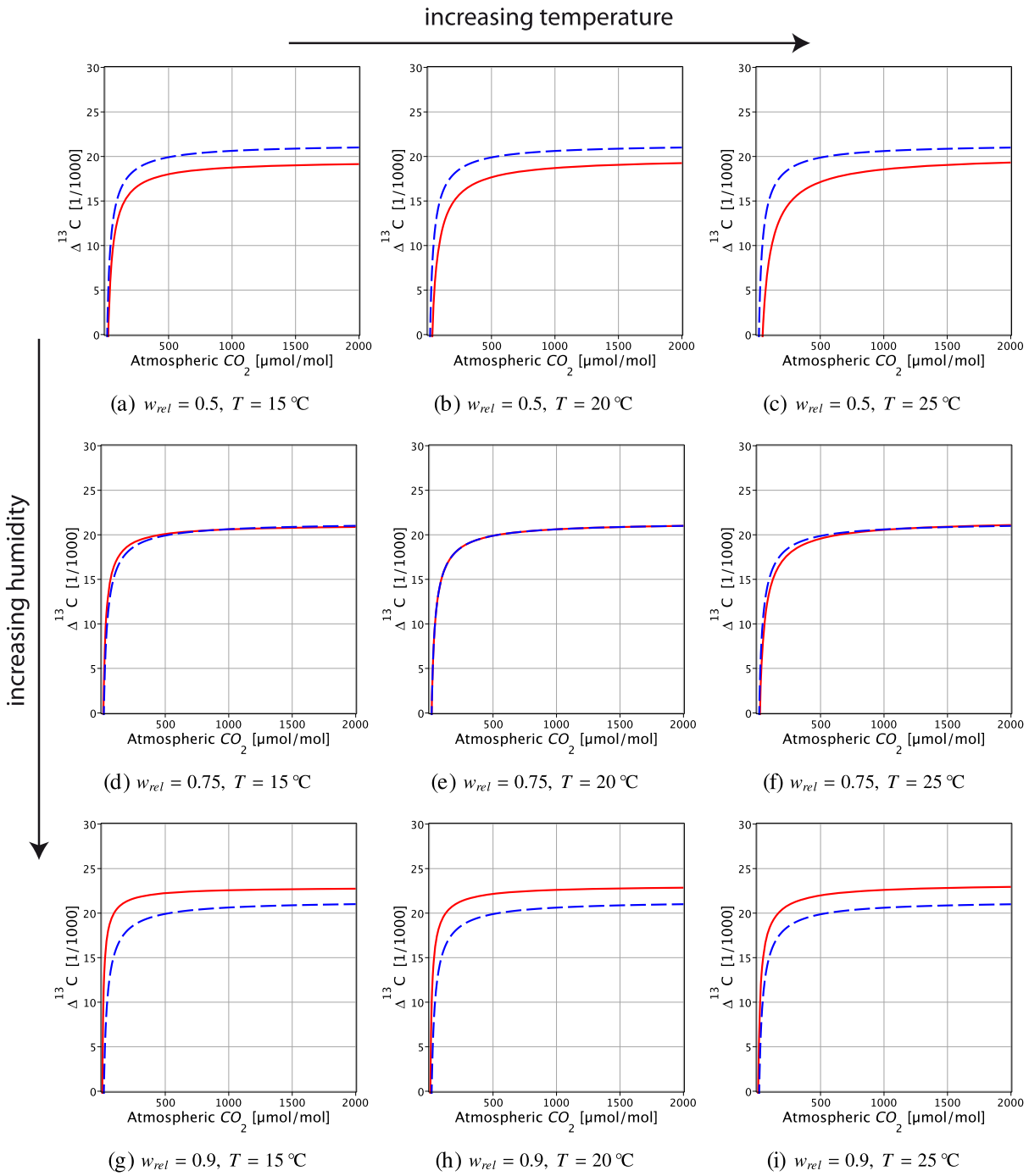

FIGURE 5 The discrimination $\Delta^{13}C$ for *G. biloba* as a function of atmospheric C_a, calculated via the optimisation model (solid red line) and the model of Schubert and Jahren (broken blue line). The red line represents $\Delta^{13}C_{mech}$, calculated according to expression (42), the blue line from inserting the parameters given in (46) (set to T = 20°C and w_{rel} = 0.75) into (32). Values of air humidity and air temperature are indicated, other input values are given in Table 1 [Color figure can be viewed at wileyonlinelibrary.com]

soil water availability (contained in λ). The phenomenologically derived discrimination $\Delta^{13}C$ of relation (32), in contrast, is assumed to depend only on C_a.

If humidity is low, as in Figure 5a–c, the model of Schubert and Jahren underpredicts C_a for a given $\Delta^{13}C$ (compared to the optimisation model). This is in accordance with and explains, at least partially, experimental results obtained by Lomax, Lake, Leng, and Jardine (2019) for Cenozoic and Mesozoic atmospheric conditions (≥1500 μmol/mol). On the other hand, if humidity is high, as in Figure 5g–i, the model of Schubert and Jahren overpredicts C_a.

For $C_a \gtrsim 500$ μmol/mol all curves in Figure 5 are very flat. Therefore, small uncertainties in experimentally obtained $\Delta^{13}C$ values are amplified to much larger uncertainties in the predicted C_a values.

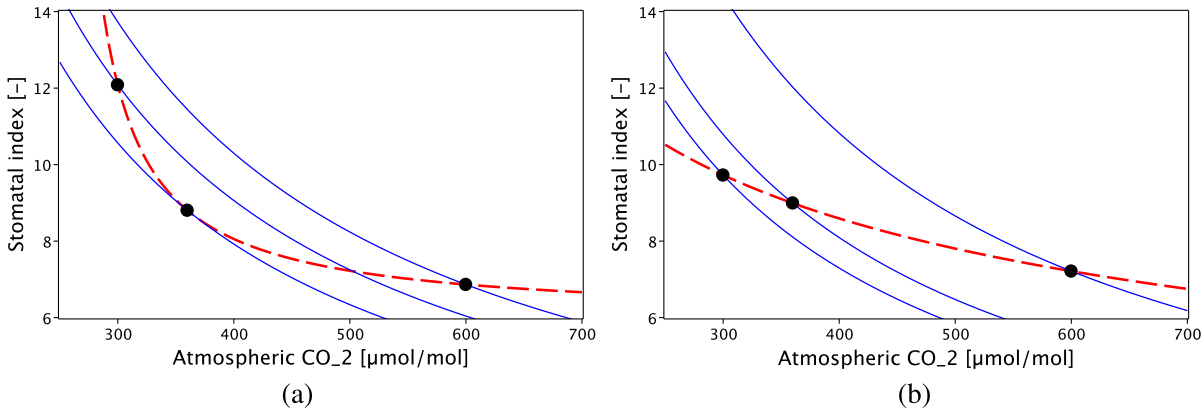

FIGURE 6 Stomatal indices vs. atmospheric CO_2-curves of *G. biloba* from (a) Royer (2001) and (b) Barclay and Wing (2016). The dashed curves represent the transfer functions $SI_{Royer} = (c - 194.4)/(0.1678\ c - 41.6)$ and $SI_{Barclay} = 113.66\ c^{-0.431}$ (c denotes the numerical value of C_a if given in units of μmol/mol). The solid curves result from application of relation (27), obtained by choosing data pairs $(C_{a,ext}, \sigma_{ext})$ (solid black circles) lying on the curves representing the transfer functions [Color figure can be viewed at wileyonlinelibrary.com]

4.2 | Fundamental problems with the stomatal ratio method

Historically, it was their seeming simplicity which made the stomatal ratio models so attractive: if one takes their simple functional form (23) (resp. (29)) for granted they contain only one unassigned and unrestricted parameter (k_{SD} resp. k_{SI}) which can be determined via relation (24) or (28) from a single known data pair $(C_{a,ext}, \nu_{ext})$ or $(C_{a,ext}, \sigma_{ext})$ obtained from plants growing under ambient CO_2 (termed 'single pair method' in the following).

Principally, this single reference data pair determines completely the functions (23) and (29) that relate C_a to ν (resp. σ), as do the structurally much more complicated mechanistic models or the transfer functions whose construction is experimentally much more laborious. This simplicity makes the stomatal ratio models indeed a tempting prospect. In what follows we will concentrate on the index-based stomatal ratio model of Section 3.2.1; the results, however, apply also to the density-based model of Section 3.2.2.

4.2.1 | Problems with the 'single pair method'

Figure 6 shows curves derived from the stomatal ratio model (via the 'single pair method' of the last paragraph) together with curves obtained via transfer functions from comprehensive data sets for *Ginkgo* (data are from Royer (2001) and Barclay and Wing (2016)). Here, the original (σ, C_a)-transfer functions constructed from these data sets by Royer (2001) and Barclay and Wing (2016) (dashed, red curves), are shown, together with several (solid, blue) curves that were calculated using relations (28) and (29). These were obtained by choosing the data pairs $(C_{a,ext}, \sigma_{ext})$, denoted by the solid black circles located upon the transfer functions.

It is obvious from Figure 6 that the (blue) curves constructed from single data pairs are not able to track the (red) experimental data sets: each data pair provides a different (blue, solid) curve, and the deviations between the transfer curve and these curves are substantial, and even (in Figure 6b) grave. In the case of Figure 6a, the solid curve (based on relation (27)) represents the transfer function in the close neighbourhood of the value $C_{a,\ ext} = 360\ \mu$mol/mol reasonably well, but this is merely a coincidence (see below), as is illustrated by Figure 6b where none of the solid curves approximates the transfer function.

Obviously, the curves produced by the stomatal ratio model cannot be viewed as valid 'local' approximations to the 'real' function $\sigma = f(C_a)$ (in this case represented by the transfer functions of Figure 6). It is worthwhile to trace this deficiency to its origin.

The starting point is equation (29) that relates C_a to σ; it is structurally extremely simple: it contains merely one undetermined parameter, k_{SI}. Once $k_{SI} = \sigma_{ext}C_{a,ext}$ has been fixed by choosing a definite point $(C_{a,ext}, \sigma_{ext})$ lying on the 'real' function $\sigma = f(C_a)$ it is guaranteed that the curve associated with (29) intersects $\sigma = f(C_a)$ at that point.

A local approximation of a function $\sigma = f(C_a)$ should represent this function not only at a single point $(C_{a,ext}, \sigma_{ext})$ but rather in a neighbourhood of this point, otherwise it is of very limited value. That is, the local approximation curve should not only intersect $\sigma = f(C_a)$, it should be also tangential to $\sigma = f(C_a)$ at $(C_{a,ext}, \sigma_{ext})$; in other words, the slope $d\sigma/dC_a = -k_{SI}/C_a^2$ of (29) and the slope df/dC_a of the real function $\sigma = f(C_a)$ should coincide for $C_a = C_{a,ext}$. To achieve this, it is imperative that expression (29) contains not only one but (at least) two undetermined parameters. Since the parameter k_{SI} is already determined by the relation $k_{SI} = \sigma_{ext}C_{a,ext}$, no parameter is left to guarantee equality of the slopes.

Thus, the extreme structural simplicity of expression (29) explains both the inability of the stomatal ratio models to serve as local approximations of unknown but nevertheless real functions $\sigma = f(C_a)$ and the inability of the 'single pair method' to reproduce realistic C_a-values. Since this deficiency is rooted in the very structure of the stomatal ratio models it is irreparable.

4.2.2 | Does it make sense to improve the statistics of the stomatal ratio method?

Obviously, the one-point calibration by one reference data pair on which the 'single pair method' is based is not robust from the viewpoint of error analysis. At first glance, fitting (23) (resp. (29)) to a higher number of already known (ν, C_a)-pairs (resp. (σ, C_a)-pairs) in order to generate data redundancy and robustness when determining k_{SD} seems to suggest itself as a tool to mitigate this problem.

But the structural problem identified in Section 4.2.1 remains. Even if k_{SI} has been determined to a high accuracy the major deficiency of Equation (29) is still present: its lack of generality cannot be rectified if one insists on its simple mathematical structure; simplicity has its price.

5 | CONCLUSION

Unsurprisingly, this survey suggests that no model is perfectly appropriate for all situations; rather, typical situations can be specified in which one of the models is superior, for example, in accuracy or ease of application, to the other ones.

Furthermore, the results of this study indicate a major conceptual gap between the mechanistic models on one side and the stomatal ratio models on the other side:

- Despite (or, more probably, because of) their seeming mathematical simplicity the stomatal ratio models suffer from inconsistencies.
- The mechanistic models, on the other hand, require much more input data than the stomatal ratio approach. For the most complex model, the optimisation approach, it may be difficult to obtain all necessary data.
- The mechanistic models and the stomatal ratio models converge for very high C_a. However, the C_a value beyond which these models show comparable predictive power may be so high that the convergence of the models is of little practical use.

The model of Schubert and Jahren features a structural deficit that produces inevitably large uncertainties if CO_2 values beyond $C_a \gtrsim 500$ μmol/mol are to be predicted.

Overall, the model of Franks et al. (2014) and the reduced order model (Konrad et al., 2017) appear to be a good compromise between applicability (which shows in the amount of the required model input) and accuracy (for which complexity is a prerequisite), even if climatic conditions such as atmospheric temperature and humidity can only be estimated.

ACKNOWLEDGEMENTS

This manuscript originated from discussions at the Special Session *Cenozoic plant diversity: gradients in time and space and their impact on early humans* (ROCEEH/NECLIME) of the EPPC 2018 in Dublin. The authors would like to thank the organisers of this NECLIME session (Angela A. Bruch, Alexandra-Jane Henrot, Louis François, Natalia Rudaya and Torsten Utescher) for the invitation to contribute to this Special Issue. This work benefitted from workshops associated with the Research Coordination Network on Cenozoic CO_2 (NSF OCE16-36005). P.J.F. was supported by the Australian Research Council. The authors would also like to thank Gabriel Katul, Nicholas School of the Environment and Earth Sciences, Duke University, Durham, United States, for helpful comments that improved the manuscript, and the reviewers for their constructive comments.

CONFLICT OF INTEREST

The authors declare no conflicts of interest.

ORCID

Wilfried Konrad https://orcid.org/0000-0002-8686-7865

REFERENCES

Aalto, T., & Juurola, E. (2002). A three-dimensional model of CO_2 transport in air-spaces and mesophyll cells of a silver birch leaf. *Plant, Cell & Environment*, *25*, 399–1409.

Ainsworth, E. A., & Rogers, A. (2007). The response of photosynthesis and stomatal conductance to rising [CO_2]: Mechanisms and environmental interactions. *Plant, Cell & Environment*, *30*, 258–270.

Anagnostou, E., John, E. H., Edgar, K. M., Foster, G. L., Ridgwell, A., Inglis, G. N., … Pearson, P. N. (2016). Changing atmospheric CO_2 concentration was the primary driver of early Cenozoic climate. *Nature*, *533*, 380–384.

Aris, R. (1975). *The mathematical theory of diffusion and reaction in permeable catalysts: The theory of the steady state* (Vol. 1). Oxford: Clarendon Press, Oxford University Press.

Barclay, R. S., & Wing, S. L. (2016). Improving the ginkgo CO_2 barometer: Implications for the early Cenozoic atmosphere. *Earth and Planetary Science Letters*, *439*, 158–171.

Beerling, D. J. (1994). Predicting leaf gas exchange and $\delta^{13}C$ responses to the past 30000 years of global environmental change. *New Phytologist*, *128*, 425–433.

Beerling, D. J., & Royer, D. L. (2002). Reading a CO_2 signal from fossil stomata. *New Phytologist*, *153*, 387–397.

Beerling, D. J., & Royer, D. L. (2011). Convergent Cenozoic CO_2 history. *Nature Geoscience*, *4*, 418–420.

Bernacchi, C. J., Pimentel, C., & Long, S. P. (2003). In vivo temperature response functions of parameters required to model RuBP-limited photosynthesis. *Plant, Cell & Environment*, *26*, 1419–1430.

Berninger, F., Mäkela, A., & Hari, P. (1996). Optimal control of gas exchange during drought: Empirical evidence. *Annals of Botany*, *77*, 469–476.

Brown, H. T., & Escombe, F. (1900). Static diffusion of gases and liquids in relation to the assimilation of carbon and translocation in plants. *Philosophical Transactions of the Royal Society B: Biological Sciences*, *193*, 223–291.

Buckley, T. N., & Schymanski, S. J. (2014). Stomatal optimisation in relation to atmospheric CO_2. *New Phytologist*, *201*, 372–377.

Cowan, I. R. (1977). Stomatal behaviour and the environment. *Advances of Botanical Research*, *4*, 117–227.

Cui, Y., & Schubert, B. A. (2016). Quantifying uncertainty of past pCO_2 determined from changes in C_3 plant carbon isotope fractionation. *Geochimica et Cosmochimica Acta*, *172*, 127–138.

Cui, Y., & Schubert, B. A. (2018). Towards determination of the source and magnitude of atmospheric pCO_2 change across the early Paleogene hyperthermals. *Global and Planetary Change*, *170*, 120–125.

De Boer, H. J., Lammertsma, E. I., Wagner-Cremer, F., Dilcher, D. L., Wassen, M. J., & Dekker, S. C. (2011). Climate forcing due to

optimization of maximal leaf conductance in subtropical vegetation under rising CO_2. *Proceedings of the National Academy of Sciences of the United States of America*, *108*, 4041–4046.

Diefendorf, A. F., Freeman, K. H., Wing, S. L., Currano, E. D., & Mueller, K. E. (2015). Paleogene plants fractionated carbon isotopes similar to modern plants. *Earth and Planetary Science Letters*, *429*, 33–44.

Farquhar, G. D., O'Leary, M. H., & Berry, J. A. (1982). On the relationship between carbon isotope discrimination and the intercellular carbon dioxide concentration in leaves. *Functional Plant Biology*, *9*, 121–137.

Farquhar, G. D., von Caemmerer, S., & Berry, J. A. (1980). A biochemical model of photosynthetic CO_2 assimilation in leaves of C_3 species. *Planta*, *149*, 78–90.

Farquhar, G. D., Von Caemmerer, S., & Berry, J. A. (2001). Models of photosynthesis. *Plant Physiology*, *125*, 42–45.

Foster, G. L., Royer, D. L., & Lunt, D. J. (2017). Future climate forcing potentially without precedent in the last 420 million years. *Nature Communications*, *8*, 14845.

Franks, P. J., Adams, M. A., Amthor, J. S., Barbour, M. M., Berry, J. A., Ellsworth, D. S., … von Caemmerer, S. (2013). Sensitivity of plants to changing atmospheric CO_2 concentration: From the geological past to the next century. *New Phytologist*, *197*, 1077–1094.

Franks, P. J., Royer, D. L., Beerling, D. J., Van de Water, P. K., Cantrill, D. J., Barbour, M. M., & Berry, J. A. (2014). New constraints on atmospheric CO_2 concentration for the Phanerozoic. *Geophysical Research Letters*, *41*, 4685–4694.

García-Amorena, I., Wagner, F., van Hoof, T. B., & Manzaneque, F. G. (2006). Stomatal responses in deciduous oaks from southern Europe to the anthropogenic atmospheric CO_2 increase; refining the stomatal-based CO_2 proxy. *Review of Palaeobotany and Palynology*, *141*, 303–312.

Grein, M., Roth-Nebelsick, A., & Wilde, V. (2010). Carbon isotope composition of middle Eocene leaves from the Messel Pit, Germany. *Palaeodiversity*, *3*, 1–7.

Hincke, A. J. C., Broere, T., Kürschner, W. M., Donders, T. H., & Wagner-Cremer, F. (2016). Multi-year leaf-level response to sub-ambient and elevated experimental CO_2 in *Betula nana*. *PLoS One*, *11*, e0157400.

Katul, G., Manzoni, S., Palmroth, S., & Oren, R. (2010). A stomatal optimization theory to describe the effects of atmospheric CO_2 on leaf photosynthesis and transpiration. *Annals of Botany*, *105*, 431–442.

Katul, G., Palmroth, S., & Oren, R. (2009). Leaf stomatal responses to vapour pressure deficit under current and CO_2-enriched atmosphere explained by the economics of gas exchange. *Plant, Cell & Environment*, *32*, 968–979.

Kleidon, A. (2007). Optimized stomatal conductance and the climate sensitivity to carbon dioxide. *Geophysical Research Letters*, 34.

Konrad, W. (2007). *Functional anatomy and biophysical mechanisms of fluid transport in vascular plants: Implications for structural optimisation in fossil and extant plants*. (PhD thesis). University of Tübingen.

Konrad, W., Katul, G., Roth-Nebelsick, A., & Grein, M. (2017). A reduced order model to analytically infer atmospheric CO_2 concentration from stomatal and climate data. *Advances in Water Resources*, *104*, 145–157.

Konrad, W., Roth-Nebelsick, A., & Grein, M. (2008). Modelling of stomatal density response to atmospheric CO_2. *Journal of Theoretical Biology*, *253*, 638–658.

Kowalczyk, J. B., Royer, D. L., Miller, I. M., Anderson, C. W., Beerling, D. J., Franks, P. J., … Ramezani, J. (2018). Multiple proxy estimates of atmospheric CO_2 from an early Paleocene rainforest. *Paleoceanography and Paleoclimatology*, *33*, 1427–1438.

Kürschner, W. M., Kvacek, Z., & Dilcher, D. L. (2008). The impact of Miocene atmospheric carbon dioxide fluctuations on climate and the evolution of terrestrial ecosystems. *Proceedings of the National Academy of Sciences*, *105*, 449–453.

Kürschner, W. M., van der Burgh, J., Visscher, H., & Dilcher, D. L. (1996). Oak leaves as biosensors of late neogene and early pleistocene paleoatmospheric CO_2 concentrations. *Marine Micropaleontology*, *27*, 299–312.

Kürschner, W. M., Wagner, F., Visscher, E. H., & Visscher, H. (1997). Predicting the response of leaf stomatal frequency to a future CO_2-enriched atmosphere: Constraints from historical observations. *Geologische Rundschau*, *86*, 512–517.

Lomax, B. H., Lake, J. A., Leng, M. J., & Jardine, P. E. (2019). An experimental evaluation of the use of $\Delta^{13}C$ as a proxy for palaeoatmospheric CO_2. *Geochimica et Cosmochimica Acta*, *247*, 162–174.

McElwain, J. C., & Chaloner, W. G. (1995). Stomatal density and index of fossil plants track atmospheric carbon dioxide in the Palaeozoic. *Annals of Botany*, *76*, 389–395.

McElwain, J. C., & Chaloner, W. G. (1996). The fossil cuticle as a skeletal record of environmental change. *PALAIOS*, *11*, 376–388.

Nobel, P. S. (2005). *Physicochemical and environmental plant physiology*. Amsterdam: Academic Press.

Parkhurst, D. F. (1994). Diffusion of CO_2 and other gases inside leaves. *New Phytologist*, *126*, 449–479.

Parlange, J.-Y., & Waggoner, P. E. (1970). Stomatal dimensions and resistance to diffusion. *Plant Physiology*, *46*, 337–342.

Poole, I. (1999). Stomatal density and index: The practice. In *Fossil plants and spores: Modern techniques* (pp. 257–260). London: The Geological Society.

Royer, D. L. (2001). Stomatal density and stomatal index as indicators of paleoatmospheric CO_2 concentration. *Review of Palaeobotany and Palynology*, *114*, 1–28.

Sack, L., & Buckley, T. N. (2016). The developmental basis of stomatal density and flux. *Plant Physiology*, *171*, 2358–2363.

Schubert, B. A., & Jahren, A. H. (2012). The effect of atmospheric CO_2 concentration on carbon isotope fractionation in C_3 land plants. *Geochimica et Cosmochimica Acta*, *96*, 29–43.

Schubert, B. A., & Jahren, A. H. (2015). Global increase in plant carbon isotope fractionation following the last glacial maximum caused by increase in atmospheric pCO_2. *Geology*, *43*, 435–438.

Steinthorsdottir, M., & Vajda, V. (2015). Early Jurassic (late Pliensbachian) CO_2 concentrations based on stomatal analysis of fossil conifer leaves from eastern Australia. *Gondwana Research*, *27*, 932–939.

Wagner, F., Below, R., Klerk, P. D., Dilcher, D. L., Joosten, H., Kürschner, W. M., & Visscher, H. (1996). A natural experiment on plant acclimation: Lifetime stomatal frequency response of an individual tree to annual atmospheric CO_2 increase. *Proceedings of the National Academy of Sciences*, *93*, 11705–11708.

Way, D. A., Oren, R., Kim, H.-S., & Katul, G. G. (2011). How well do stomatal conductance models perform on closing plant carbon budgets? A test using seedlings grown under current and elevated air temperatures. *Journal of Geophysical Research: Biogeosciences*, *116*.

Woodward, F. I. (1987). Stomatal numbers are sensitive to increases in CO_2 from pre-industrial levels. *Nature*, *327*, 617–618.

Wynn, J. G. (2003). Towards a physically based model of CO_2-induced stomatal frequency response. *New Phytologist*, *157*, 394–398.

How to cite this article: Konrad W, Royer DL, Franks PJ, Roth-Nebelsick A. Quantitative critique of leaf-based paleo-CO_2 proxies: Consequences for their reliability and applicability. *Geological Journal*. 2020;1–17. https://doi.org/10.1002/gj.3807